The evolution of hadron spectra in the modified leading logarithm approximation

S. Albino[1], B. A. Kniehl[1], G. Kramer[1], W. Ochs[2]

[1] Institut für Theoretische Physik, Universität Hamburg, Luruper Chaussee 149, 22761 Hamburg, Germany
[2] Max-Planck-Institut für Physik (Werner-Heisenberg-Institut), Föhringer Ring 6, 80805 München, Germany

Abstract. We perform fits of $\Lambda_{\rm QCD}$ and the gluon fragmentation function $D(x, Q)$ at initial scale $Q_0 \gg \Lambda_{\rm QCD}$ to charged light hadron momentum spectra data by evolving in the modified leading logarithm approximation. Without additional assumptions, we achieve a good description of the available data for $\xi = \ln(1/x)$ up to and around the Gaussian peak, and values of $\Lambda_{\rm QCD}$ acceptably close to those in the literature. In particular, we find that this procedure describes the position of the peak, and, in contrast to the limiting spectrum, also the normalization.

1 Introduction

Cross sections in which hadrons are detected in the final state currently cannot be reliably calculated from first principles in quantum chromodynamics (QCD). However, as a result of the factorization theorem, one can separate these cross sections into perturbatively calculable hard parts convoluted with parton densities if there are hadrons in the initial state and fragmentation functions (FFs), which contain all the information on the soft transition from a parton a to the produced hadron h. FFs for charged particles have been well determined over large and intermediate values of the hadronic momentum fraction $x = 2p/\sqrt{s}$, where p is the momentum of the hadron h and $\sqrt{s}$ is the center-of-mass energy, by fitting to a wealth of experimental data [1]. However, data at $x < 0.1$ have always been excluded from fits because the convergence of the fixed order perturbation series for the evolution of the FFs is spoilt by terms of the form $\alpha_{\rm s}^n \ln^m(1/x)$, and so FFs are not well understood at small x. A theory which resums these logarithms at leading and sub-leading order exists – the modified leading logarithm approximation (MLLA) [2] (for reviews see [3,4]). The MLLA is a systematic improvement over an earlier approximation, the double logarithmic approximation (DLA), which resums leading logarithms by summing tree level diagrams in which the outgoing gluons are strongly ordered in their angles of emission, thereby giving the largest logarithm of the gluon FF at the order in $\alpha_{\rm s}$ of the diagram [5].

The MLLA has been primarily studied in the context of the local parton–hadron duality (LPHD) approach [6]. Here, one assumes that, when the longitudal momentum fraction z of the observed hadron relative to the parent parton is low, a sufficiently inclusive hadronic process has

similar properties to the corresponding process involving partons with transverse momentum less than the order of the hadron's mass. The FFs describe all partons with transverse momentum less than the factorization scale Q, so for light hadron production the shape in x space of the initial FFs with initial factorization scale $Q_0 = O(\Lambda_{\rm QCD})$ will be similar to the shape of the probability for a parton to emit a parton, i.e. these FFs are delta functions in $(1 - z)$, and only the absolute normalization K_h is undetermined. Using this assumption, and fixing $Q_0 = \Lambda_{\rm QCD}$, where the MLLA resummed evolution is well behaved, leads to the so-called limiting spectrum [7,8] which can make predictions for data at small x with just two free parameters to be fitted, K_h and $\Lambda_{\rm QCD}$. Together with the conventional choice $Q = \sqrt{s}/2$, this approach has been very successful at describing the $\xi = \ln(1/x)$ dependence of small x data, provided some modifications are made to the MLLA evolved normalization: in [8] an additional component not provided by the MLLA was added, whereas in [9] a different K_h was fitted for each value of $\sqrt{s}$.

In this paper, we are interested in studying MLLA evolution without using strong assumptions about the non-perturbative physics such as the LPHD, or modifying the MLLA evolution itself. There are a number of important reasons for this. Firstly, it is interesting to determine whether the MLLA can describe the $\sqrt{s}$ dependence of the overall normalization of the data. Secondly, in current analyses, where only the NLO calculation has been used, such as in [1], fitting is achievable only to data for which $x \gtrsim 0.1$ ($\xi \lesssim 2.3$). A continued rise in the data as x decreases is predicted, whereas the experimental data reach a peak and then fall. Therefore it is important to know if one can use the MLLA to improve the hard part at small x such that the fitting can be extended over that in the

literature to include data for which $x < 0.1$ and therefore, since the cross section depends on the FFs for $z \geq x$, obtain the FFs in that region. Thirdly, using weaker assumptions will allow for a purer test of the MLLA and determine its kinematic range of validity better. This can be achieved, as in global fits, by taking $Q_0 \gg \Lambda_{\rm QCD}$ to stay in the perturbative region, in which case one does not need to assume the limiting spectrum to be valid, and absorbing the soft physics at energy scales less than Q_0 into a parameterized FF, whose free parameters can be fitted to data at Q by evolving this initial FF in the MLLA. The distorted Gaussian in ξ, with no MLLA evolution, gives a good description of data over the range of $Q \gg \Lambda_{\rm QCD}$ [7,10], so we shall employ this parameterization at $Q = Q_0$.

The organization of this work is as follows. In Sect. 2 we shall repeat the basic MLLA equation in moment space and discuss various approximations to it. Section 3 contains the comparison with e^+e^- single charged hadron spectra at the larger scale $Q > Q_0$ and the determination of $\Lambda_{\rm QCD}$. In Sect. 4 we make some changes to the theoretical input to further understand the limitations of our general approach. Finally, in Sect. 5 we present our conclusions.

2 MLLA evolution

Before we present our results concerning the evolution of the low x spectra based on the MLLA evolution equations, we shall list the basic equations on which our analysis rests. We work in the LO approximation where the inclusive cross section for $e^+e^- \rightarrow hX$ as a function of x is related to the FFs $D_q^h(x,Q)$ for the transitions $q \rightarrow h$ and $\bar{q} \rightarrow h$ by

$$\frac{1}{\sigma_{\rm tot}} \frac{{\rm d}\sigma^h}{{\rm d}x} = \frac{\sum_q e_q^2 D_q^h(x,Q)}{\sum_q e_q^2}, \tag{1}$$

where e_q is the electoweak charge on quark q, $\sigma_{\rm tot} = N_c \sum_q 4\pi e_q^2 \alpha^2/(3s)$ is the total cross section, and σ^h is the cross section for the inclusive production of a hadron h.

As usual we also use the variable ξ. At sufficiently small x, i.e. large ξ, the contribution to the cross section from the non-singlet sector may be neglected in our approach since the non-singlet evolution is free from small x logarithms. Writing each quark FF in the form

$$D_q^h(x,Q) = D_\Sigma^h(x,Q) + D_{{\rm NS},q}^h(x,Q), \tag{2}$$

where the singlet $D_\Sigma^h(x,Q)$ is defined to be the sum over all quark FFs divided by the number of quark flavors N_f and the $D_{{\rm NS},q}^h(x,Q)$ are the non-singlets, we therefore see that each quark FF in (1) may be replaced by the singlet FF. Furthermore, at small x one can make the approximation, good within MLLA accuracy, that the singlet FF is related to the gluon FF by

$$D_\Sigma^h(x,Q) = \frac{2C_F}{N_c} D_g^h(x,Q), \tag{3}$$

where $C_F = (N_c^2 - 1)/(2N_c)$. Using these approximations in (1), we find that the cross section in the MLLA can

be written

$$\frac{1}{\sigma_{\rm tot}} \frac{{\rm d}\sigma^h}{{\rm d}x} = \frac{2C_F}{N_c} D_g^h(x,Q). \tag{4}$$

In other words, for describing the fragmentation $q(\bar{q}) \rightarrow h$ at large ξ we can just use the FF for $g \rightarrow h$. Note therefore that the cross section can only depend on N_f through the evolution of the gluon FF, which we will consider just now. In the following we shall skip the upper and lower indices and write $D_g^h(x,Q) = D(x,Q)$. The MLLA equation for $D(x,Q)$ is most easily written by introducing the moment transform $D_j(Q)$ of $D(x,Q)$, which is

$$D_j(Q) = \int_0^1 {\rm d}x x^{j-1} D(x,Q), \tag{5}$$

with the inverse transformation

$$D(x,Q) = \int_{\tau-i\infty}^{\tau+i\infty} \frac{{\rm d}j}{2\pi i} x^{-j} D_j(Q), \tag{6}$$

where τ must be chosen such that the integration contour lies to the right of all poles in $D_j(Q)$. We introduce $\omega = j - 1$ and write $D_\omega(Y) = D_j(Q)$ with $Y = \ln(Q/Q_0)$. Then the MLLA equation for $D_\omega(Y)$ is [3]

$$\left(\omega + \frac{{\rm d}}{{\rm d}Y}\right) \frac{{\rm d}}{{\rm d}Y} D_\omega(Y) - 4N_c \frac{\alpha_{\rm s}}{2\pi} D_\omega(Y)$$

$$= -a\left(\omega + \frac{{\rm d}}{{\rm d}Y}\right) \frac{\alpha_{\rm s}}{2\pi} D_\omega(Y), \tag{7}$$

where $a = 11N_c/3 + 2N_f/(3N_c^2)$. The solution to this equation for $D_\omega(Y)$ is weakly dependent on N_f. Indeed, as shown in [8], the moments of the data calculated with $N_f = 3$ and those calculated with N_f increasing by unity whenever $\sqrt{s}$ is large enough for the contribution from a heavy quark flavor to become relevant give similar results up to $\sqrt{s} = 202$ GeV within the error range on the moments extracted from the experimental data. This observation is also substantiated by a recent experimental analysis [11], where it was found that at the Z^0 resonance, where the effect of heavy quark production is maximal, the ξ spectra at the peak determined for all flavors differs from the one for just the light flavors by about 8%. In analyses using the limiting spectrum it has been sufficient for all available data to set $N_f = 3$, and we will therefore use this value throughout this paper. By introducing the anomalous dimension $\gamma_\omega(\alpha_{\rm s})$, we have

$$D_\omega(Y) = D_\omega(0) \exp\left\{\int_0^Y {\rm d}y \gamma_\omega(\alpha_{\rm s}(y))\right\}. \tag{8}$$

If $D_\omega(0)$ is known from the FF at the starting scale Q_0, which must be taken from experimental data, (8) gives us the solution for arbitrary Y, if we know $\gamma_\omega(\alpha_{\rm s})$. Equation (7) is equivalent to the following differential equation for γ_ω:

$$(\omega + \gamma_\omega)\gamma_\omega - 4N_c \frac{\alpha_{\rm s}}{2\pi} \tag{9}$$

$$= -\beta(\alpha_{\rm s})\frac{{\rm d}}{{\rm d}\alpha_{\rm s}}\gamma_\omega - a(\omega + \gamma_\omega)\frac{\alpha_{\rm s}}{2\pi} + ab\left(\frac{\alpha_{\rm s}}{2\pi}\right)^2,$$

where

$$\beta(\alpha_{\mathrm{s}}) = \frac{\mathrm{d}}{\mathrm{d}Y}\alpha_{\mathrm{s}}(Y) = -b\frac{\alpha_{\mathrm{s}}^2}{2\pi}, \tag{10}$$

with $b = 11N_c/3 - 2N_f/3$. The first term on the right hand side of (9) originates from the running of α_{s}. The second term gives the hard single-logarithmic correction to the DLA soft emission. The last term is formally a next-to-MLLA term, which may be neglected. A general solution of (7) in terms of confluent hypergeometric functions is known [3, 7]. Equivalently, one can solve (9) in terms of Whittaker functions. However, since the MLLA equation is only valid in the region $\alpha_{\mathrm{s}} \ll 1$ and $\omega = O(\sqrt{\alpha_{\mathrm{s}}})$, we can obtain a simpler but equally accurate solution to (9) by expanding in $\alpha_{\mathrm{s}}/\omega \ll 1$ while keeping $\alpha_{\mathrm{s}}/\omega^2 = O(1)$ fixed,

$$\gamma_\omega = \sum_{n=1}^{\infty} \left(\frac{\alpha_{\mathrm{s}}}{\omega}\right)^n g_n\left(\frac{\alpha_{\mathrm{s}}}{\omega^2}\right), \tag{11}$$

and solving for each term. The first and second term will then resum double and single logarithms respectively, but the higher terms obtained this way will be incomplete since the MLLA does not treat terms in γ_ω which are of $O(\alpha_{\mathrm{s}}^{3/2})$ or higher in the region of validity given above.

The DLA corresponds to the $n = 1$ term, only, in (11), in which case the terms in (9) proportional to $\beta(\alpha_{\mathrm{s}})$ and a can be neglected. One obtains two solutions:

$$\gamma_\omega^\pm = \frac{1}{2}\left(-\omega \pm \sqrt{\omega^2 + 4\gamma_0^2}\right), \tag{12}$$

with

$$\gamma_0^2 = 4N_c\frac{\alpha_{\mathrm{s}}}{2\pi}. \tag{13}$$

For $\alpha_{\mathrm{s}} \to 0$ we obtain

$$\gamma_\omega^+ = \frac{\gamma_0^2}{\omega} = \frac{4N_c}{\omega}\frac{\alpha_{\mathrm{s}}}{2\pi}, \quad \gamma_\omega^- = -2\omega, \tag{14}$$

i.e. γ_ω^+ has the familiar singularity $\sim 1/\omega$ which determines the small x behavior of $D(x, Q)$ in the leading logarithm approximation (LLA). Therefore the correct solution in the DLA is $\gamma_\omega = \gamma_\omega^+$. This solution is finite for $\omega \to 0$ and is equal to $\gamma_0 \sim \sqrt{\alpha_{\mathrm{s}}}$.

Once the solution for the $n = 1$ term in (11) has been chosen, there is only one solution for the $n = 2$ term, and we have finally

$$\gamma_\omega = \frac{1}{2}\left(-\omega + \sqrt{\omega^2 + 4\gamma_0^2}\right)$$
$$+ \frac{\alpha_{\mathrm{s}}}{2\pi}\left[b\frac{\gamma_0^2}{\omega^2 + 4\gamma_0^2} - \frac{a}{2}\left(1 + \frac{\omega}{\sqrt{\omega^2 + 4\gamma_0^2}}\right)\right]$$
$$+ O\left(\left(\frac{\alpha_{\mathrm{s}}}{\omega}\right)^3\frac{\alpha_{\mathrm{s}}}{\omega^2}\right). \tag{15}$$

This approximate solution is usually referred to as the MLLA result [3]. The term proportional to a modifies the $\alpha_{\mathrm{s}} \to 0$ limit to

$$\gamma_\omega = \left(\frac{4N_c}{\omega} - a\right)\frac{\alpha_{\mathrm{s}}}{2\pi}, \tag{16}$$

which reproduces the finite correction to the LO γ_ω^+ in the LLA. The result in (15) must be substituted in (8) to obtain the corresponding MLLA solution for $D_\omega(Y)$. Writing

$$D_\omega(Y) = D_\omega(0)\widetilde{D}_\omega(Y), \tag{17}$$

we have

$$\ln\widetilde{D}_\omega(Y) = \int_0^Y \mathrm{d}y\,\gamma_\omega(\alpha_{\mathrm{s}}(y)). \tag{18}$$

Using the LO formula $\alpha_{\mathrm{s}}(y) = 2\pi/[b(y + \lambda)]$, where we introduce $\lambda = \ln(Q_0/\Lambda_{\mathrm{QCD}})$, the integration in (18) with γ_ω given in (15) yields

$$\ln\widetilde{D}_\omega(Y) = f(\omega, Y, \lambda) - f(\omega, 0, \lambda), \tag{19}$$

where

$$f(\omega, Y, \lambda) = -\frac{1}{2}Z + \frac{1}{2}\sqrt{Z(Z + 4A)}$$
$$+ (2A - B)\ln\left(\sqrt{Z + 4A} + \sqrt{Z}\right)$$
$$+ \left(\frac{1}{4} - \frac{B}{2}\right)\ln Z - \frac{1}{4}\ln(Z + 4A). \tag{20}$$

In (20) we introduced $A = 4N_c/(b\omega)$, $B = a/b$ and $Z = \omega(Y + \lambda)$. Then the solution $\widetilde{D}_\omega(Y)$ can be written as

$$\widetilde{D}_\omega(Y) = \mathrm{e}^{f(\omega, Y, \lambda) - f(\omega, 0, \lambda)}, \tag{21}$$

with

$$\mathrm{e}^{f(\omega, Y, \lambda)} = \mathrm{e}^{-\frac{1}{2}Z + \frac{1}{2}\sqrt{Z(Z + 4A)}}\left[\sqrt{Z + 4A} + \sqrt{Z}\right]^{2A - B}$$
$$\times \left(\frac{Z}{Z + 4A}\right)^{\frac{1}{4}}Z^{-\frac{B}{2}}. \tag{22}$$

By fixing Λ_{QCD} the evolution of $D_\omega(Y)$ is completely determined by (21) and (22). This solution has for $Y \to \infty$ the following asymptotic behavior:

$$\mathrm{e}^{f(\omega, Y, \lambda)} \simeq Z^{A-B}. \tag{23}$$

In [3, 12] it was found that for $\omega \gtrsim 1$, γ_ω in the MLLA accidentally mimics the behavior of the LLA LO γ_ω reasonably well. This is aided by the observation that the $\omega \to \infty$ limit of (15) is equal, up to terms of $O(1/\omega)$, to that of (16), the α_{s}, $\omega \to 0$ limit of the LLA LO γ_ω, whose $O(\omega)$ corrections turn out to be rather unimportant at $\omega = O(1)$ and negative at large ω. Therefore we neglect those corrections beyond MLLA which are important at small ξ.

Solving (9) for the $n = 3$ term of (11) gives us a contribution to the next-to-MLLA correction which reads

$$\gamma_\omega^{\mathrm{NMLLA}} = \left(\frac{\alpha_{\mathrm{s}}}{\omega}\right)^3 g_3\left(\frac{\alpha_{\mathrm{s}}}{\omega^2}\right)$$
$$= \left(\frac{\alpha_{\mathrm{s}}}{2\pi}\right)^2\left[a^2\frac{\gamma_0^2}{(\omega^2 + 4\gamma_0^2)^{\frac{3}{2}}}\right.$$

$$+ \frac{ab}{2} \left(\frac{1}{\sqrt{\omega^2 + 4\gamma_0^2}} - \frac{\omega^3}{(\omega^2 + 4\gamma_0^2)^2} \right) \quad (24)$$

$$+ b^2 \left(\frac{2\gamma_0^2}{(\omega^2 + 4\gamma_0^2)^{\frac{3}{2}}} - \frac{5\gamma_0^4}{(\omega^2 + 4\gamma_0^2)^{\frac{5}{2}}} \right) \Biggr].$$

The addition of this term to the expression in (15) would give a more accurate approximation to the exact solution to (9) if (11) were a suitably convergent series. However, these results are not complete at next-to-MLLA order; in particular they refer only to gluon jets. In the complete next-to-MLLA cross section both the evolution and (3) obtain a correction, the latter arising from the energy dependent differences between quark and gluon jets [13]. In any case, we can at least use the term in (24) to determine the stability of our form for the MLLA evolution in different regions of ξ and $\sqrt{s}$.

Finally, since partons are treated as massless in the MLLA, the parton momentum spectrum is equivalent to the parton energy spectrum. Consequently the MLLA formalism needs modification in order to incorporate hadron mass effects, which become more relevant as ξ increases. However, such effects will be neglected in our analysis since otherwise model assumptions are needed.

3 Fitting the experimental data

In this section we test how well the MLLA described in the previous section agrees with experimental data, both by fitting free parameters to data sets and by using the resulting fitted parameters to predict other data sets.

$\Lambda_{\rm QCD}$ is the only parameter on which MLLA evolution depends, and should therefore be obtainable by fitting to data at widely separated energies, starting from TASSO data at $Q_0 = 14\,{\rm GeV}/2$ [14]. Therefore we use data at the highest $\sqrt{s}$, namely the recent data at $\sqrt{s} = 202\,{\rm GeV}$ from OPAL [9], as well as data at $91\,{\rm GeV}$ [15] from the same collaboration, which have the highest accuracy. For all experimental data used in this paper, systematic and statistical errors are added in quadrature. As in [9], we impose a lower bound on the OPAL data of

$$\xi > 0.75 + 0.33 \ln \left(\sqrt{s}/{\rm GeV} \right) \quad (25)$$

since at lower ξ the experimental errors are too small to fit using only one parameter. Including these small ξ points in fact does not change the results significantly but leads to a much higher minimized χ^2. To control the number of data used in the non-perturbative region of hadronic momentum $p = O(\Lambda_{\rm QCD})$, we introduce a cut-off mass scale m and impose an upper limit on the data used of $p > m$, or

$$\xi < \ln \frac{\sqrt{s}}{2m}. \quad (26)$$

The initial gluon FF used for this fit was obtained by independently fitting it to data at the lowest $\sqrt{s}$, namely the TASSO data at $\sqrt{s} = 14\,{\rm GeV}$, using a distorted Gaussian,

$$xD(x, Q_0) = \frac{N}{\sigma\sqrt{2\pi}} \quad (27)$$

Table 1. Fit of a distorted Gaussian to all 20 TASSO data points at $\sqrt{s} = 14\,{\rm GeV}$ with $Q_0 = \sqrt{s}/2$

Parameter	N	$\bar{\xi}$	σ^2	s	k
Value	9.71	2.33	0.61	−0.11	−0.77
Error	0.11	0.01	0.02	0.05	0.12

$$\times \exp\left[\frac{1}{8}k - \frac{1}{2}s\delta - \frac{1}{4}(2+k)\delta^2 + \frac{1}{6}s\delta^3 + \frac{1}{24}k\delta^4 \right],$$

where $\delta = (\xi - \bar{\xi})/\sigma$ and $Q_0 = 14\,{\rm GeV}/2$, and the results are shown in Table 1. The errors were obtained from the diagonal components of the inverted matrix of second derivatives of χ^2 at the minimum. Since this method assumes that χ^2 is quadratic in the parameters, these errors should not be taken too seriously. In this case there was no need to impose a lower ξ bound on the TASSO data since there were 5 free parameters in the fit. We also imposed no upper ξ bound on this data, since doing so either made little difference for $m \lesssim 0.5\,{\rm GeV}$ or did not constrain the parameters sufficiently for $m \gtrsim 0.5\,{\rm GeV}$. The achieved χ^2 per degree of freedom, $\chi^2_{\rm DF}$, is 0.76, and the results in Table 1 for the parameters of the distorted Gaussian fit agree well with earlier fits in the literature [16].

The resulting values of $\Lambda_{\rm QCD}$ when performing this procedure, and cutting the data using values of m ranging from 0.3 to 0.6 GeV, are shown in Table 2, where it can be seen that the obtained value for $\Lambda_{\rm QCD}$ with $N_f = 3$ depends somewhat on the upper limit for ξ. The errors were calculated by varying $\Lambda_{\rm QCD}$, in both directions, from its value at the minimum until χ^2 increased by unity. The errors were found to be symmetric and close to the inverse of the second derivative of χ^2 with respect to $\Lambda_{\rm QCD}$. If we choose the $\Lambda_{\rm QCD}$ from the fit with the smallest $\chi^2_{\rm DF}$ we have $\Lambda_{\rm QCD} = 317\,{\rm MeV}$ in reasonable agreement with LO $\Lambda_{\rm QCD}$ values with $N_f = 3$ obtained in other analyses [8,16].

The fits for $m = 0.3$ and $0.6\,{\rm GeV}$ are shown graphically in Figs. 1 and 2. These figures also show the predictions of the respective fits for TPC data at $29\,{\rm GeV}$ [17], TASSO data at 35 and $44\,{\rm GeV}$ [14], TOPAZ data at $58\,{\rm GeV}$ [18] and OPAL data at 133 [19] and $172\,{\rm GeV}$ [20]. In all plots in this paper, each curve is shifted up from the curve below by 0.8 for clarity. The data are well described almost up to the peak, about one half or one unit in ξ below. Beyond the peak the predictions fail.

In [8] a much better agreement with data over the whole ξ range was obtained, but the MLLA prediction was modified in two aspects. Firstly, an energy independent background term was added to the MLLA multiplicity formula and, secondly, a correction for mass effects at large ξ was

Table 2. Four independent fits of $\Lambda_{\rm QCD}$ to OPAL data at 91 and 202 GeV, where the cuts in each case are labelled by the value of m

m (GeV)	0.3	0.4	0.5	0.6
$\Lambda_{\rm QCD}$ (MeV)	258 ± 8	293 ± 9	307 ± 10	317 ± 10
$\chi^2_{\rm DF}$	7.0	3.0	2.3	1.8
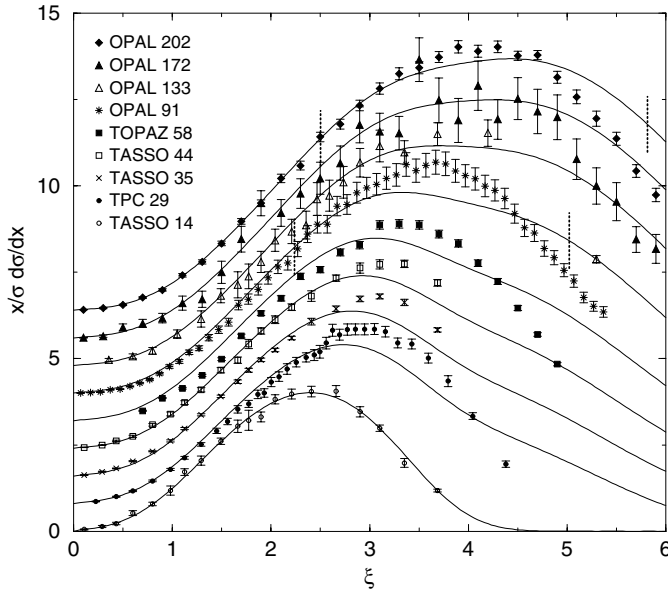
Fig. 1. Fit of Λ_{QCD} to OPAL data at $\sqrt{s} = 91$ and $202\,\mathrm{GeV}$, after fitting the initial gluon FF to TASSO data at $14\,\mathrm{GeV}$. The ξ region of data is chosen as described in (25) and (26), and is indicated by the vertical dotted lines. The upper bound corresponds to $m = 0.3\,\mathrm{GeV}$. The predictions from this fit of other data sets is also shown. The lowest curve shows the independent distorted Gaussian fit to TASSO data at $14\,\mathrm{GeV}$. Each curve is shifted up by 0.8 for clarity

added. In contrast, our fit, starting from the Gaussian parameterization of the TASSO data at $14\,\mathrm{GeV}$, predicts the ξ distributions at higher energies using only a single parameter, Λ_{QCD}; it is remarkable that MLLA evolution predicts all data sets at higher energies very well up to the peak region. The discrepancy beyond the peak region in our case is too large to be attributed to mass effects.

The distorted Gaussian parameters are highly correlated with one another, so in order to constrain them better, we fit these parameters and Λ_{QCD} simultaneously to TASSO data at $14\,\mathrm{GeV}$ and OPAL data at 91 and $202\,\mathrm{GeV}$. We again impose the upper bound of (26), but this time on all three data sets for consistency. However, we impose no lower bound on any of the data, because all distorted Gaussian parameters are free in the fit. Taking first $m = 0.4\,\mathrm{GeV}$, we obtained the results presented in Table 3 with $\chi^2_{\mathrm{DF}} = 2.3$, which are shown graphically in Fig. 3. This figure also contains predictions for other data sets not used in the fit. The case for $m = 0.5\,\mathrm{GeV}$ is shown in Table 4 and Fig. 4, where $\chi^2_{\mathrm{DF}} = 2.1$. Since the dependence of χ^2 on the parameters cannot be adequately approximated by a quadratic, and since the present study does not aim at a precise determination of Λ_{QCD}, we refrain from calculating the errors in these and subsequent tables.

The data around the peak region are better described for $m = 0.5\,\mathrm{GeV}$. We note that there is a large difference between the parameters in each case, which may be due to the fact that the theory cannot accomodate some or all of the three main features of the data, being the position of the maximum, the width and the normalization. Indeed, two local minima were found in each fit, and the global
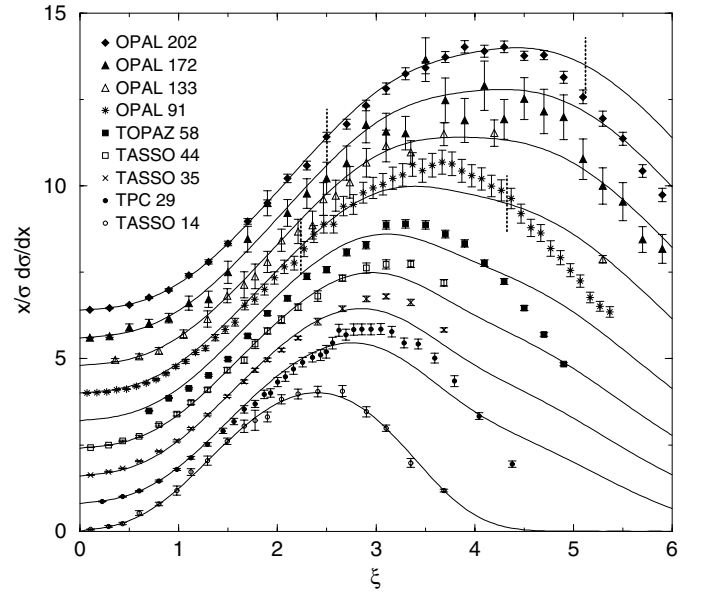
Fig. 2. As in Fig. 1, with an upper bound in ξ on the data used corresponding to $m = 0.6\,\mathrm{GeV}$ and indicated by a vertical dotted line. Each curve is shifted up by 0.8 for clarity. (Note again that the lowest curve is from an independent fit to all TASSO data at $\sqrt{s} = 14\,\mathrm{GeV}$, and hence is identical to the corresponding curve in Fig. 1.)

Table 3. Fit of gluon FF and Λ_{QCD} to all TASSO data at $14\,\mathrm{GeV}$ and OPAL data at 91 and $202\,\mathrm{GeV}$ (88 data points), with $m = 0.4\,\mathrm{GeV}$

N	$\bar{\xi}$	σ^2	s	k	Λ_{QCD} (MeV)
7.86	2.11	0.40	-0.46	-1.32	649
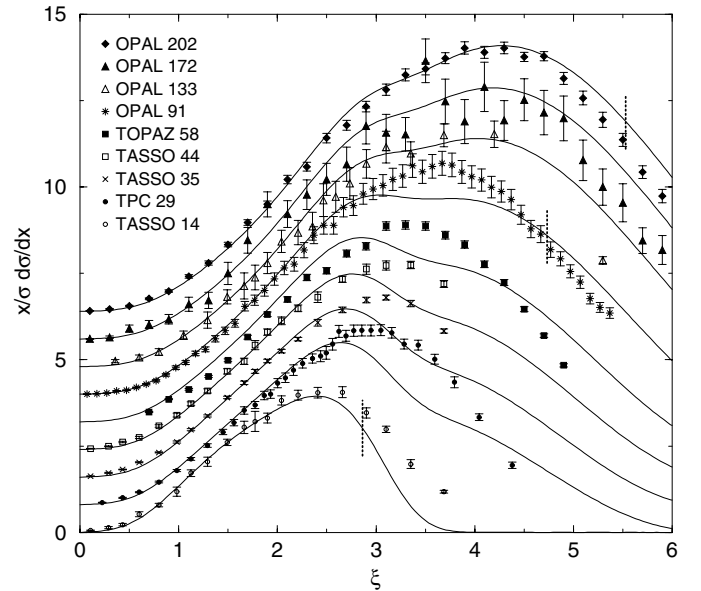
Fig. 3. Fit of gluon FF and Λ_{QCD} to TASSO data at $14\,\mathrm{GeV}$ and OPAL data at 91 and $202\,\mathrm{GeV}$, with an upper bound in ξ on the data used corresponding to $m = 0.4\,\mathrm{GeV}$ and indicated by a vertical dotted line. Other data sets are shown for comparison. The upper bound on ξ for each data set used in the fit is indicated by a vertical dotted line

Table 4. As in Table 3, but with 83 data points and $m = 0.5\,\mathrm{GeV}$

N	$\bar{\xi}$	σ^2	s	k	Λ_{QCD} (MeV)
11.80	2.60	0.67	-0.26	-1.48	87

Table 5. Fit to all available data (413 data points), with $m = 0.5\,\mathrm{GeV}$ (see text)

N	$\bar{\xi}$	σ^2	s	k	Λ_{QCD} (MeV)
11.65	2.57	0.70	-0.19	-1.17	130
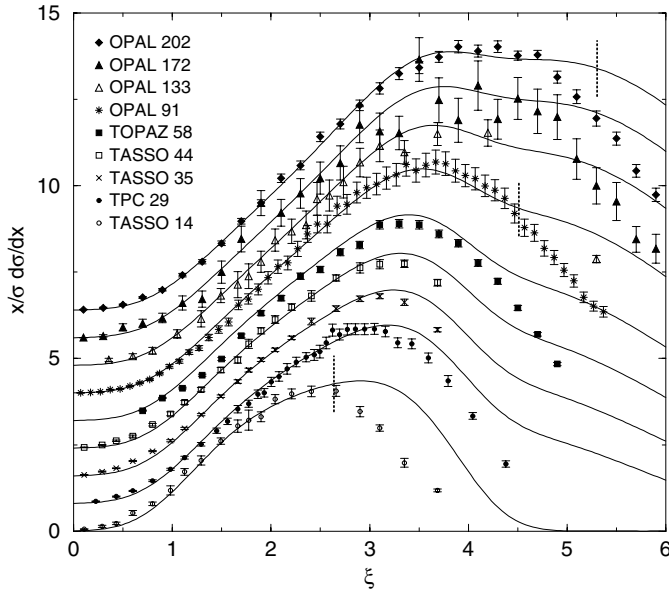
Fig. 4. As in Fig. 3, but with $m = 0.5\,\mathrm{GeV}$

Fig. 5. Global fit of gluon FF and Λ_{QCD}, with $m = 0.5\,\mathrm{GeV}$, to the data shown here and other data listed in the text

minimum shifted from one of these two local minima to the other as m increased from 0.4 to 0.5 GeV.
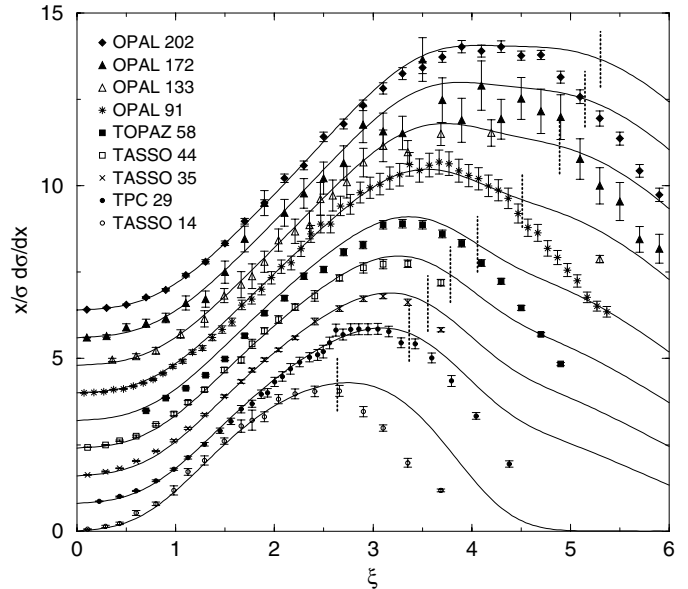
The resulting values for Λ_{QCD} in the fits of Tables 3 and 4 are clearly too different for either of them to be taken seriously. This is probably due to the fact that Λ_{QCD} and the distorted Gaussian parameters are highly correlated with one another. In the fits of Table 2, the values of Λ_{QCD} are more consistent with each other since they were completely uncorrelated with the distorted Gaussian parameters.

To better constrain all the parameters would require using more data sets in the fit. Therefore we fit the distorted Gaussian parameters and Λ_{QCD} to all available data sets, namely the data sets in Figs. 1–4, as well as TASSO data at 22 GeV [21], ALEPH [22], DELPHI [23], L3 [24] and SLD [25] data at 91 GeV, ALEPH data at 133 GeV [26], DELPHI data at 161 GeV [27] and OPAL data at 183 and 189 GeV [20]. For $m = 0.5$ GeV, we obtained the results shown in Table 5 and Fig. 5, for which $\chi^2_{\mathrm{DF}} = 4.0$ was achieved. The results do not differ significantly from those in Table 4 and Fig. 4, nor from similar fits with $m = 0.4$ and 0.6 GeV, for which we obtained $\Lambda_{\mathrm{QCD}} = 106$ and 129 MeV respectively. In all cases we found that there were more than one local minimum, from which we selected the minimum with the smallest χ^2.

The fit in Fig. 5 is the main result of this paper. A global fit in which the parameters of the distribution at the lowest scale Q_0 are fitted simultaneously with the parameter Λ_{QCD} leads to an improvement over the fits in Figs. 1 and 2. At all energies the description is now good up to the peak or even beyond. We stress again that this fit, beyond the input parameterization at Q_0, does not involve any additional assumptions beyond the MLLA evolution.

4 Further studies

In all our fits so far we obtained a good description of the data below the maximum, i.e. for small ξ values, but a rather bad description in the region above the peak, i.e. for large ξ (with the exception of the TASSO 14 GeV data, when it was fitted over the whole ξ range). This discrepancy may have several reasons.

Since the MLLA approach is supposed to be particularly valid for sufficiently large ξ, presumably in the peak region, despite the discussion at the end of Sect. 2 it may have been necessary to exclude data below a given ξ, e.g. that of (25), in our approach of fitting the distorted Gaussian parameters and Λ_{QCD} simultaneously to all three data sets. However, with this approach only a few data points are left, in particular for the TASSO data at 14 GeV, when imposing also the upper limit on ξ in (26). Therefore a lower ξ cut with the approach applied in Tables 3 and 4 does not work.

Alternatively, it may be that the upward evolution of the higher moments tends to become unstable. To investigate this possibility, we fit the distorted Gaussian parameters and Λ_{QCD} to TASSO data at 14 GeV and OPAL data at 91 and 202 GeV as before, but this time we set $Q_0 = 202\,\mathrm{GeV}/2$, i.e. we fit the initial distribution at the highest energy and evolve downwards. The results of this fit are

Table 6. Fit of gluon FF to TASSO data at 14 GeV and OPAL data at 91 and 202 GeV (83 data points), using $Q_0 = 202\,\mathrm{GeV}/2$ and downward evolution, with $m = 0.5\,\mathrm{GeV}$

N	$\bar{\xi}$	σ^2	s	k	Λ_{QCD} (MeV)
26.83	3.66	1.17	−0.52	−1.49	225
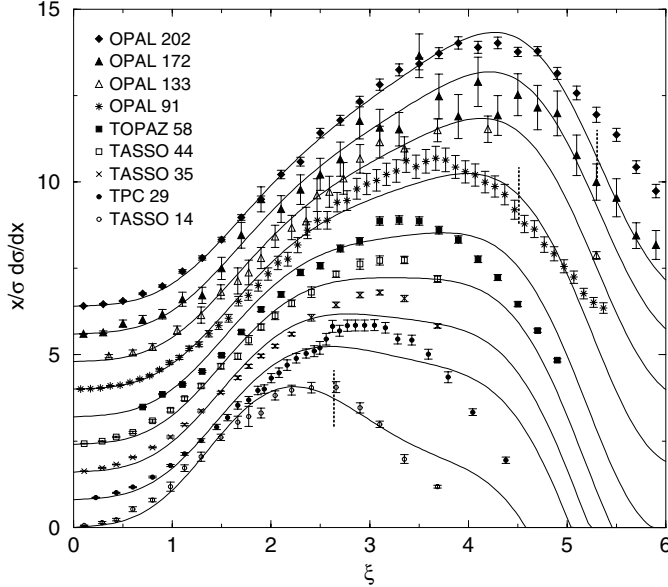
Fig. 6. Fit of gluon FF to TASSO data at 14 GeV and OPAL data at 91 and 202 GeV, using $Q_0 = 202\,\mathrm{GeV}/2$ and downward evolution, with $m = 0.5\,\mathrm{GeV}$

shown in Table 6 and Fig. 6, where $\chi^2_{\mathrm{DF}} = 3.9$. The value of Λ_{QCD} obtained is in good agreement with that obtained in other analyses. The resulting ξ distributions also fit better to the data at the highest energies at larger ξ values beyond the peak, whereas at the remaining energies the description of the data around the peak becomes worse.

Another possibility for our large ξ discrepancy may be due to the region of function space in ξ available to the parameterization in (27) being insufficient. To enlarge this region, we add a term

$$C_5\delta^5 + C_6\delta^6 \qquad (28)$$

to the argument of the exponential in (27), and include C_5 and C_6 in the list of parameters to be fitted. However, when performing this fit with $m = 0.5\,\mathrm{GeV}$, there is no significant improvement over the fit in Fig. 4.

This indicates that the failure to describe the region above the peak is inherent to the MLLA formalism as it is applied here. A better approximation to the full analytic solution to (7) may improve the large ξ description, since it includes certain corrections of next-to-MLLA order. Such corrections are also included, for example, in the limiting spectrum within the LPHD approach, where, compared to our fits, a better description of the data beyond the peak is achieved, given suitable modifications to the MLLA evolution of the normalization (see Sect. 1). Therefore we repeated the fit of Fig. 4, but this time including the extra term given by (24) in the evolution. In this case χ^2_{DF}

increased to 2.6, and this increase can be attributed to the fact that the deviations from the data were slightly larger beyond the peak. However, up to the peak the description was as good as the fit of Fig. 4. Furthermore the theoretical curves were rather similar to those of Fig. 4 in the ξ range of the data. This suggests that the MLLA can only describe data up to the peak, and that a full next-to-MLLA calculation is required beyond the peak, which includes, in particular, the correlation between the evolution of quark and gluon jets.

5 Conclusions

In this work we perform fits to the available momentum spectra data of e^+e^- annihilation in the energy range 14–202 GeV using MLLA evolution. No additional assumptions, such as the LPHD, is used other than a conjectured functional form for the gluon FF, and therefore we have achieved a particularly pure test of the MLLA. We find a good description of the data in the region up to the maximum of the distribution in the scaling variable ξ, with only a minimal number of parameters. In particular we find that MLLA evolution without additional input gives a good description of the normalization up to the peak, and also the approximate position of the peak.

Our fitted values of Λ_{QCD} cover a large range. However, in our model-independent approach, there is some theoretical ambiguity in Λ_{QCD}. We have chosen the renormalisation and factorization scales to be $Q = \sqrt{s}/2$, but we could also have chosen some factor of this, of $O(1)$. With this theoretical error, our results for Λ_{QCD} are consistent with those of other studies [1,8,9,16].

Clearly, our form for the MLLA evolution is insufficient to describe the data above the peak. The inclusion of the next-to-MLLA contribution, (24), does not improve our results. At this order, a full treatment of momentum distributions would include quark–gluon mixing, which may be the most important effect at this order and therefore may significantly help to reduce the large ξ discrepancy.

Finally, it will be interesting to incorporate the MLLA into the full NLO fits which apply to the large x range, in order to extend the region of validity towards lower values of x. Our recipe for fitting the fragmentation functions is consistent and compatible with the standard fitting.

References

1. B.A. Kniehl, G. Kramer, B. Pötter, Nucl. Phys. B **582**, 514 (2000); S. Kretzer, Phys. Rev. D **62**, 054001 (2000); L. Bourhis, M. Fontannaz, J.P. Guillet, M. Werlen, Eur. Phys. J. C **19**, 89 (2001)

2. Yu.L. Dokshitzer, S.I. Troyan, Report No. LENINGRAD-84-922 (1984)
3. Yu.L. Dokshitzer et al., Basics of perturbative QCD (Editions Frontières, Gif-sur-Yvette, 1991)
4. V.A. Khoze, W. Ochs, Int. J. Mod. Phys. A **12**, 2949 (1997)
5. B.I. Ermolaev, V.S. Fadin, JETP Lett. **33**, 269 (1981); V.S. Fadin, Sov. J. Nucl. Phys. **37**, 245 (1983); A.H. Mueller, Nucl. Phys. B **213**, 85 (1983)
6. Ya.I. Azimov, Yu.L. Dokshitzer, V.A. Khoze, S.I. Troyan, Z. Phys. C **27**, 65 (1985)
7. Yu.L. Dokshitzer, V.A. Khoze, S.I. Troyan, Int. J. Mod. Phys. A **7**, 1875 (1992)
8. S. Lupia, W. Ochs, Eur. Phys. J. C **2**, 307 (1998)
9. G. Abbiendi et al. [OPAL Collaboration], Eur. Phys. J. C **27**, 467 (2003)
10. C.P. Fong, B.R. Webber, Nucl. Phys. B **355**, 54 (1991)
11. K. Abe et al. [SLD Collaboration], Phys. Rev. D **69**, 072003 (2004)
12. Yu.L. Dokshitzer, V.A. Khoze, S.I. Troyan, Z. Phys. C **55**, 107 (1992); J. Phys. G **17**, 1481 (1991)
13. A.H. Mueller, Nucl. Phys. B **241**, 141 (1984); E.D. Malaza, B.R. Webber, Phys. Lett. B **149**, 501 (1984)
14. W. Braunschweig et al. [TASSO Collaboration], Z. Phys. C **47**, 187 (1990)
15. M.Z. Akrawy et al. [OPAL Collaboration], Phys. Lett. B **247**, 617 (1990)
16. N.H. Brook, I.O. Skillicorn, Phys. Lett. B **479**, 173 (2000)
17. H. Aihara et al. [TPC/Two Gamma Collaboration], Phys. Rev. Lett. **61**, 1263 (1988)
18. R. Itoh et al. [TOPAZ Collaboration], Phys. Lett. B **345**, 335 (1995)
19. G. Alexander et al. [OPAL Collaboration], Z. Phys. C **72**, 191 (1996)
20. G. Abbiendi et al. [OPAL Collaboration], Eur. Phys. J. C **16**, 185 (2000)
21. M. Althoff et al. [TASSO Collaboration], Z. Phys. C **22**, 307 (1984)
22. R. Barate et al. [ALEPH Collaboration], Phys. Rept. **294**, 1 (1998)
23. P. Abreu et al. [DELPHI Collaboration], Z. Phys. C **73**, 11 (1996)
24. B. Adeva et al. [L3 Collaboration], Phys. Lett. B **259**, 199 (1991)
25. K. Abe et al. [SLD Collaboration], Phys. Rev. D **59**, 052001 (1999)
26. D. Buskulic et al. [ALEPH Collaboration], Z. Phys. C **73**, 409 (1997)
27. K. Ackerstaff et al. [OPAL Collaboration], Z. Phys. C **75**, 193 (1997)